

Submitted to Scripta Materialia (revised January 2016)

## **Shear fracture mechanism in micro-tension of an ultrafine-grained pure copper using synchrotron radiation X-ray tomography**

Jianwei Li <sup>a,b</sup>, Jie Xu <sup>a,b,\*</sup>, Bin Guo <sup>a,b</sup>, Debin Shan <sup>a,b</sup>, Terence G. Langdon <sup>c,d</sup>

<sup>a</sup> Key Laboratory of Micro-systems and Micro-structures Manufacturing of Ministry of Education, Harbin Institute of Technology, Harbin 150080, China

<sup>b</sup> School of Materials Science and Engineering, Harbin Institute of Technology, Harbin 150001, China

<sup>c</sup> Departments of Aerospace & Mechanical Engineering and Materials Science, University of Southern California, Los Angeles, CA 90089-1453, USA

<sup>d</sup> Materials Research Group, Faculty of Engineering and the Environment, University of Southampton, Southampton SO17 1BJ, UK

### **Abstract**

In order to investigate the early fracture of ultrafine-grained (UFG) pure copper with a partially recrystallized microstructure and simple shear texture, the evolution of surface strain was measured using *in situ* micro-tension with digital image correlation. The spatial distribution of voids in tensile specimens was revealed after testing using synchrotron radiation X-ray tomography. The results show that the shear fracture behavior is associated with void evolution in UFG copper and this is strongly affected by the simple shear texture produced by equal-channel angular pressing (ECAP). The results have important implications for use in micro-forming.

**Keywords:** equal-channel angular pressing; fracture; micro-forming; synchrotron X-ray tomography; ultrafine grains.

Corresponding author: [xjhit@hit.edu.cn](mailto:xjhit@hit.edu.cn) (J. Xu)

Ultrafine-grained (UFG) materials with large fractions of high-angle grain boundaries and high strength are advantageous for use in micro-forming since the size effects, such as process scatter and uneven shape evolution, can be significantly reduced by comparison with conventional coarse-grained (CG) materials [1-4]. At the same time, however, the low ductility of UFG materials during tension has attracted significant attention [5, 6]. This poor ductility is associated with a change in deformation behavior and the introduction of shear localization due to the exceptional grain refinement in UFG materials [7]. Although several strategies have been proposed to improve the poor ductility of UFG materials [8-10], the fracture mechanism of UFG materials is at present not well defined [11]. For example, it was suggested that the fracture mechanism after necking depends mainly on the presence of inclusions [5] and recently shear fracture was reported as the common feature of UFG materials fabricated by equal-channel angular pressing (ECAP) [12] or high-pressure torsion (HPT) [13]. It is reasonable to anticipate, therefore, a correlation between the shear texture produced by ECAP or HPT processing and the subsequent fracture behavior. The present investigation was initiated specifically to reveal the nature of the shear fracture mechanism during the non-homogenous deformation of UFG Cu processed by ECAP and subsequently tested in micro-tension.

The experiments were conducted using pure copper (99.9%) having a bimodal structure with a simple shear texture which was composed of fine/ultrafine grains of  $\sim 0.4 \mu\text{m}$  and coarse grains of  $\sim 3.5 \mu\text{m}$  [14]. Billets were processed by ECAP at

room temperature using route Bc in which the sample is rotated by  $90^\circ$  in the same sense between each pass [15]. Each billet was pressed through a total of 12 passes using a die with an internal channel angle,  $\Phi$ , of  $110^\circ$  so that each separate pass imposed a strain of  $\sim 0.8$  [16]. Miniature tensile specimens with nominal gauge dimensions of  $1.0 \times 1.0 \times 0.5 \text{ mm}^3$  were electro-discharge machined from the cross-sections of the ECAP billets. With the billet positioned as it exits the outlet channel, the three orthogonal directions were  $X$  which is normal to the side plane between the top and bottom edges,  $Y$  which is along the length of the billet and  $Z$  which is normal to the top plane of the billet: these directions and the orientations of the tensile specimens are shown in Fig. 1(a).

The miniature tensile specimens were ground on SiC papers up to 2400 until very thin lines were achieved along the loading direction. The surface was then evenly sprayed using a very thin layer of white paint and a coating of carbon dust was placed on the surface to provide image contrast for digital image correlation (DIC). An *in situ* tensile test was conducted using a Kammrath-Weiss micro-tensile stage with a nominal strain rate of  $1 \times 10^{-4} \text{ s}^{-1}$  within an optical microscope (OM) having a magnification of  $\times 80$ . Each tensile test was conducted two times to confirm the reproducibility. The surface images were recorded after every  $5 \text{ }\mu\text{m}$  of displacement and analyzed using the VIC-2D DIC measurement system (Correlated Solutions, Inc.) in order to calculate the surface strain in the loading direction. The specimens fracture surface was also observed by scanning electron microscopy (SEM) using an FEI Co. Quanta 200F.

Selected specimens were subjected to synchrotron radiation X-ray tomography at a true strain of  $\sim 0.22$  after the peak stress. For these observations, it was necessary to use thinned tensile specimens of 0.4 mm thickness because of the high X-ray absorption in pure copper. It should be noted, however, that the use of these thin specimens will have little effect on the fracture behavior due to the decreasing specimen thickness for specimens with ultrafine grains [17]. These experiments were performed using the BL13W1 beam line at the Shanghai Synchrotron Radiation Facility (SSRF) with a voxel size of  $0.27 \mu\text{m}^3$ . With this resolution, it was possible to observe voids as small as  $\sim 1.0 \mu\text{m}$ . Thus, even smaller voids are not included in the 3D analysis but it is reasonable to assume they will have no significant influence on the fracture behavior.

The true stress-true strain curve of UFG pure copper reveals three regimes as shown in Fig. 1(a): an initial elastic stage, a narrow domain of plastic deformation up to an ultimate tensile stress of  $\sim 385 \text{ MPa}$  and then strain softening with further strain. The surface strain analysis areas in Fig. 1(b) exhibit the severely inhomogeneous deformation. Strain localization zones are mainly concentrated in the center of the specimen and become gradually denser with increasing strain. It is obvious that the inclination of the strain localization zone is at about  $45^\circ$  with respect to the loading axis, where this angular inclination is typical for pure metals. In Fig. 1(c) the plot of local strain vs. distance shows that the highest local strain zone is concentrated within the distance from  $\sim 0.68$  to  $\sim 0.86 \text{ mm}$  and this remains dense starting at a true strain of  $\sim 0.037$  until fracture. The highest local strain up to  $\sim 0.5$  contributes to the total true

strain at  $\sim 0.242$ . There is also another lower local strain peak at a distance of  $\sim 1.04$  mm which shows a slower growth rate. Thus, the appearance of multiple strain peaks suggests an incompatibility between shear bands for UFG pure copper. This also means that the extreme true strain for uniform plastic deformation is  $\sim 0.037$  or even earlier and not the peak stress at  $\sim 0.075$  when the strain localization or the shear bands become more obvious in Fig. 1(b).

Figure 2 shows typical images of the fracture characteristics of (a) coarse-grained (CG) and (b) – (h) UFG pure copper from three planes X, Y, and Z, which are perpendicular to the directions X, Y and Z, respectively. Clearly, Fig. 2 (a) and (b) show the fracture mode of UFG copper is very different from that for CG copper. It is important to note that the fracture plane in Fig. 2 (c) with an angle of  $\sim 55^\circ$  in the X plane is consistent with a shear angle of  $\Phi/2 = 55^\circ$  for a die angle of  $110^\circ$  parallel to the shear plane for the final ECAP pass. Similar results were obtained for the fatigue fracture behavior for UFG copper during tension [12] and the tension fracture of UFG nickel processed by HPT [13]. This finding demonstrates that the fracture mode is strongly associated with the simple shear texture produced by ECAP. It is very similar to the fracture of pure magnesium with a rolled texture during tension [18]. Many inner voids are formed near the fracture surface after tension and an example is enlarged in Fig. 2 (d). Importantly, this crack path from the void edge to the crack tip gradually increases to  $\sim 55^\circ$  parallel with the fracture angle. The shear bands all tend to have a similar inclination angle of  $\sim 45^\circ$  along the loading axis in Fig. 2 (e) which may explain the multi-peaks of local strain in Fig. 1 (c)

due to a more severe shear deformation between the shear bands than within the shear bands. Furthermore, the deformation between shear bands leads to a localized crack path from one void to another as in Fig. 2 (f). This is consistent with the surface strain evolution in Fig. 1 (b). However, the angle of the fracture plane at  $\sim 80^\circ$  is between the angles of the shear plane ( $\sim 90^\circ$ ) and the shear bands ( $\sim 45^\circ$ ) on the  $Y$  plane in Fig. 2 (b). In the  $Z$  plane, nearly every dimple with an inclusion, as in Fig. 2 (g), exhibits a typical ductile fracture surface. Inspection of the fracture surface in Fig. 2 (h) reveals two types of areas: smooth areas and rough areas corresponding to transgranular fracture and intergranular fracture, respectively. The inhomogeneous microstructure may lead to a part shear band mechanism in the UFG region during deformation. Thus, the crack growth is greatly influenced by microstructural inhomogeneities due to the dependence on grain size according to the conventional Hall-Petch relationship.

In order to investigate the fracture behavior during micro-tension, detailed 3D representations of void features are shown in Fig. 3 and Appendix 1 after necking at a strain of  $\varepsilon = 0.22$ . The results indicate that many voids are concentrated in the necking zone when viewed on the  $X$  plane as in Fig. 3 (a) and (b). The voids in the different regions qualitatively correspond to the local strain endured by the specimen during micro-tension. A higher local strain leads to more and larger voids with some coalescence, where the volume density and the number of voids are up to  $\sim 18\%$  and  $\sim 51$ , respectively. By contrast, the lower local strain region has many relatively smaller voids, where the volume density and the number of voids are only  $\sim 0.14\%$

and 17, respectively. It is important to comment on the orientations of the voids shown in Fig. 3 (b). Most of these voids have ellipsoidal shapes with their long axes nearly parallel to the yellow thin dashed line. The growth of two representative voids is shown in Fig. 3 (c) (Marked 1 and 2) and they are consistent with the crack propagation direction in Fig. 2 (d). This suggests that the shear texture may have a strong effect on the propagation of the voids. A 3-D X-ray  $\mu$ -CT of a deformed specimen at  $\varepsilon \approx 0.22$  exhibits mainly two kinds of void coalescence in Fig. 3 (b). Most of the voids are at  $55^\circ$  along the loading direction (Marked 3) which is consistent with the fracture angle in Fig. 2 (c). The others are nearly normal to the loading direction (Marked 4). Moreover, the voids appear to be reasonably evenly distributed in the necking region when viewed from the  $Y$  plane in Fig. 3 (d). Clearly, the elongated axes of some of the voids are parallel with the surface cracks as in Fig. 2(f) and others are aligned in the loading direction.

To elucidate the fracture behavior of the UFG pure copper, a qualitative discussion based on the effects of the simple shear texture on the void formation and coalescence mechanisms is presented in Fig. 4. For the UFG pure copper with partial recrystallized microstructure produced by ECAP processing, the main deformation mechanisms during micro-tension are dislocation slip for the coarse grains and grain boundary sliding for the ultrafine grains [19,20]. It appears that the ideal  $A/\bar{A}$  and  $B/\bar{B}$  shear textures make the geometrical condition of  $\langle 110 \rangle$  closely aligned for the activation of the relatively easy  $(111)\langle 110 \rangle$  slip system in f.c.c. materials. Thus, the shear strain produced in the shear plane during the

micro-tension is larger than in any other planes. It is well known that the stress concentration due to the incompatible strain between the matrix and the inclusions, as in Fig. 2 (g) leads to void formation. During this process, the inclusions or obstacles may be the nanoscale grains due to the Hall-Petch relationship or areas with low dislocation storage capacity in the ultrafine grains. Also, due to the grain boundary spatial distribution caused by the shear deformation produced by ECAP processing, the voids tend to be easily initiated at grain boundaries and triple junctions [11] due to the advent of grain boundary sliding in UFG pure copper. Once nucleated, the void shape grows preferentially with the orientation of the major axis aligned at an angle of  $\sim 55^\circ$  by the easier shear deformation with respect to the thickness direction as in Fig. 2 (d). These two main deformation mechanisms show that the shear plane has the highest density of voids in the tensile specimen as in Fig 3 (a) and (b).

Although this kind of fracture is shear fracture, the fracture mechanism is a dimple fracture having high stress triaxiality [21]. Previous results show that the most important metallurgical parameter is the void spacing [22] for this type of fracture. The void spacing between larger voids at the lower strain area can be seen in the earlier state of the necking zone, and the direction of  $\sim 55^\circ$  along the tensile axis has the shortest average void spacing of  $\sim 71 \mu\text{m}$  of all directions in the X plane. In the severe necking zone, the advent of most of the void coalescence along  $55^\circ$  proves that the main fracture mechanism is the void sheet mechanism between two larger voids as in Fig. 3 (b). However, it is different from the fracture mode of coarse-grained pure copper with pre-existing voids by internal necking [23,24] which

is probably attributed to the microstructure. Moreover, the large void coalescence can also be seriously enhanced by shear deformation as well as microscopic shear localization between pairs of voids in the shear plane [23], which produces many small dimples between the large dimples as in Fig. 2 (g).

An appropriate criterion of void coalescence may be used in an extended form as [25-27]:

$$\frac{\sigma_n}{\sigma_y} = (1 - \chi^2) \left[ \alpha_{Th} \left( \frac{1 - \chi}{\chi W} \right)^2 + \frac{1.24}{\sqrt{\chi}} \right] \quad (1)$$

where  $\sigma_n$  is the overall stress component normal to the localization plane,  $\sigma_y$  is the yield stress,  $\chi$  and  $W$  are the effective void spacing and effective void aspect ratio, respectively, and the parameter  $\alpha_{Th}$  depends on the strain hardening exponent  $n$  as proposed by the relationship:  $\alpha_{Th} = 0.1 + 0.217n + 4.83n^2$  [27]. Eq. (1) states that void coalescence begins when  $\sigma_n$  reaches a critical value and this value decreases as two voids with nearly the same aspect ratio are close to each other. Accordingly, the nearest voids (a, b and d) in the same shear plane are naturally inclined to become more easily coalescent than other voids due to the shorter crack propagation path as shown in Fig. 3 (b). Based on this analysis, void growth and coalescence are mainly localized in the shear plane resulting from the shear texture and this turns the shear plane into the preferential fracture plane.

Thus, this simple shear texture plays an obviously accelerating role in the early fracture of UFG materials during micro-tension and this has two important implications. First, it may be possible to promote the ductility by weakening the

texture intensity during the fabrication of SPD materials. Second, this may provide a straightforward guide for the ductile fracture model.

In summary, the low ductility of UFG pure copper is due to severe strain localization, including in shear banding, which is caused by the inhomogenous microstructure. Using X-ray tomography observations, it appears that the shape and distributed spatial distribution of the voids are strongly affected by the shear texture produced by ECAP processing. The shear plane with the maximum density of voids becomes the preferential fracture plane for the early fracture of these UFG materials. A proposed 3D model provides a reasonable and consistent explanation for the shear fracture behavior induced by the simple shear texture observed in these UFG samples.

### **Acknowledgements**

This work was supported by the National Natural Science Foundation of China under Grant No. 51375111. Partial support was provided by the European Research Council under ERC Grant Agreement No. 267464-SPDMETALS. The authors thank the Shanghai Synchrotron Radiation Facility (SSRF) for provision of synchrotron radiation facilities. We also thank Dr. Guohua Fan, Mr. Meng Huang and all staff members of the BL13W1 beam line of SSRF for their assistance during the synchrotron experiments.

## References

- [1] N. Warthi, P. Ghosh, A.H. Chokshi, *Scripta Mater.* 68 (2013) 225–228..
- [2] J. Xu, X. Zhu, D. Shan, B. Guo, T.G. Langdon, *Mater. Sci. Eng. A* 636 (2015) 352–360.
- [3] J. Xu, J. Li, L. Shi, D. Shan, B. Guo, *Mater. Charact.* 109 (2015) 181–188.
- [4] J. Xu, X. Zhu, D. Shan, B. Guo, T.G. Langdon, *Adv. Eng. Mater.* 636 (2015) 352–360.
- [5] G.B. Rathmayr, R. Pippan, *Scripta Mater.* 66 (2012) 507–510.
- [6] A. Vinogradov, I.S. Yasnikov, H. Matsuyama, M. Uchida, Y. Kaneko, Y. Estrin, *Acta Mater.* 106 (2016) 295–303.
- [7] D. Jia, K.T. Ramesh, E. Ma, *Acta Mater.* 51 (2003) 3495–3509.
- [8] Y. Wang, M. Chen, F. Zhou, E. Ma, *Nature*, 419 (2002) 912-915.
- [9] Y.H. Zhao, Y.T. Zhu, X.Z. Liao, Z. Horita, and T.G. Langdon, *Appl. Phys. Lett.* 89 (2006) 121906.
- [10] Y.H. Zhao, J.F. Bingert, Y.T. Zhu, X.Z. Liao, R.Z. Valiev, Z. Horita, T.G. Langdon, Y.Z. Zhou, E.J. Lavernia, *Appl. Phys. Lett.* 92 (2008) 081903.
- [11] A. Hohenwarter, R. Pippan, *Scripta Mater.* 64 (2011) 982–985.
- [12] M. Goto, S.Z. Han, T. Yamamoto, J. Kitamura, J.H. Ahn, T. Yakushiji, S.S. Kim, J. Lee, *Int. J. Fatigue*, 92 (2016) 577–587.
- [13] M. Haddad, Y. Ivanisenko, E. Courtois-Manara, H. Fecht, *Mater. Sci. Eng. A* 620 (2015) 30–35.
- [14] J. Xu, J. Li, D. Shan, B. Guo, *Mater. Sci. Eng. A* 664 (2016) 114–125.

- [15] M. Furukawa, Y. Iwahashi, Z. Horita, M. Nemoto, T.G. Langdon, *Mater. Sci. Eng. A* 257 (1998) 328-332.
- [16] Y. Iwahashi, J. Wang, Z. Horita, M. Nemoto, T.G. Langdon, *Scripta Mater.* 35 (1996) 143-146.
- [17] Y.H. Zhao, Y.Z. Guo, Q. Wei, A.M. Dangelewicz, C. Xu, Y.T. Zhu, T.G. Langdon, Y.Z. Zhou, E.J. Lavernia, *Scripta Mater.* 59 (2008) 627–630
- [18] A. Hosokawa, D.S. Wilkinson, J. Kang, E. Maire, *Acta Mater.* 61 (2013) 1021–1036.
- [19] M.J. Nemcko, D.S. Wilkinson, *Mater. Sci. Eng. A* 676 (2016) 146–155.
- [20] T. Mungole, P. Kumar, M. Kawasaki, T.G. Langdon, *J. Mater. Sci.* 50 (2015) 3549–3561.
- [21] K.V. Ivanov, E.V. Naydenkin, *Scripta Mater.* 66 (2012) 511–514.
- [22] Y. Bao, Ph.D. Thesis, Massachusetts Institute of Technology, 2003.
- [23] A.A. Benzerga, J. Besson, A. Pineau, *J. Eng. Mater-T. ASME.* 121 (1999) 221–229.
- [24] M.J. Nemcko, J. Li, D.S. Wilkinson, *J. Mech. Phys. Solids.* 95 (2016) 270–283
- [25] T. Pardoen, J.W. Hutchinson, *J. Mech. Phys. Solids.* 48 (2000) 2467–2512.
- [26] F. Scheyvaerts, P. Onck, C. Tekoglu, T. Pardoen, *J. Mech. Phys. Solids.* 59 (2011) 373–397.
- [27] F. Hannard, T. Pardoen, E. Maire, C. Le Bourlot, R. Mokso, A. Simar, *Acta Mater.* 103 (2016) 558–572.

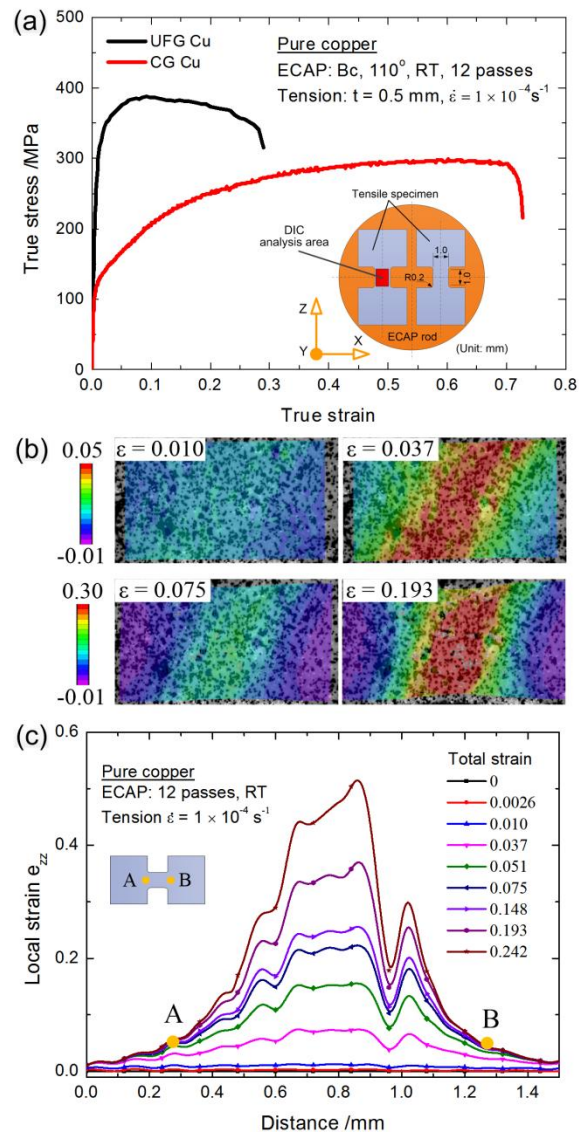


Figure 1. (a) The true stress-true strain curves with inserted tensile specimen dimensions, (b) strain in the surface distributions and (c) distributions from the longitudinal direction at different strain stages during in situ tension testing of the UFG pure copper

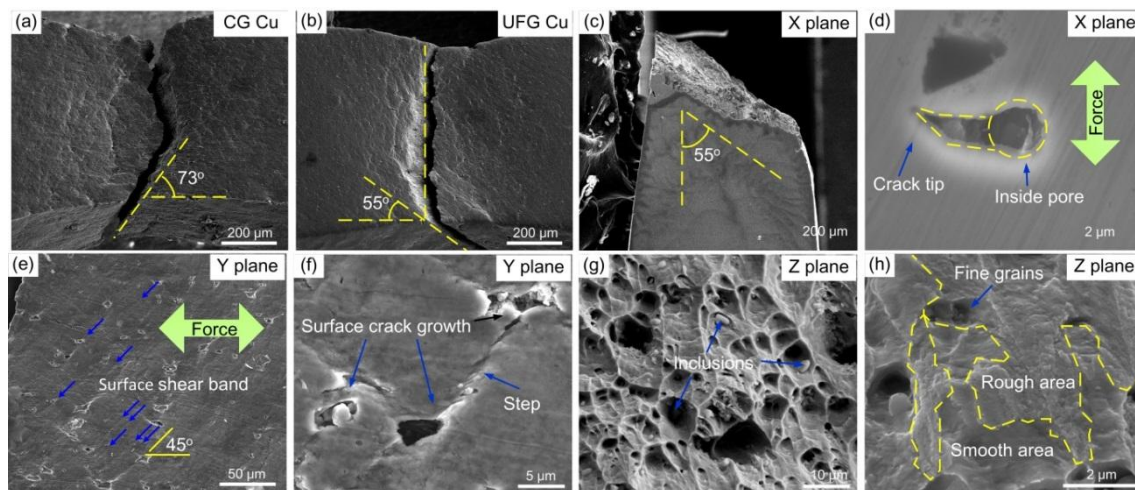


Figure 2. Typical images depicting the fracture characteristics of (a) CG pure copper and (b) UFG pure copper from three sides: (c) the fracture angle and (d) inside void from the X plane; (e) inclusions in the void and (f) ultrafine grains from the Z plane; (g) surface shear band and (h) crack growth from the Y plane, respectively.

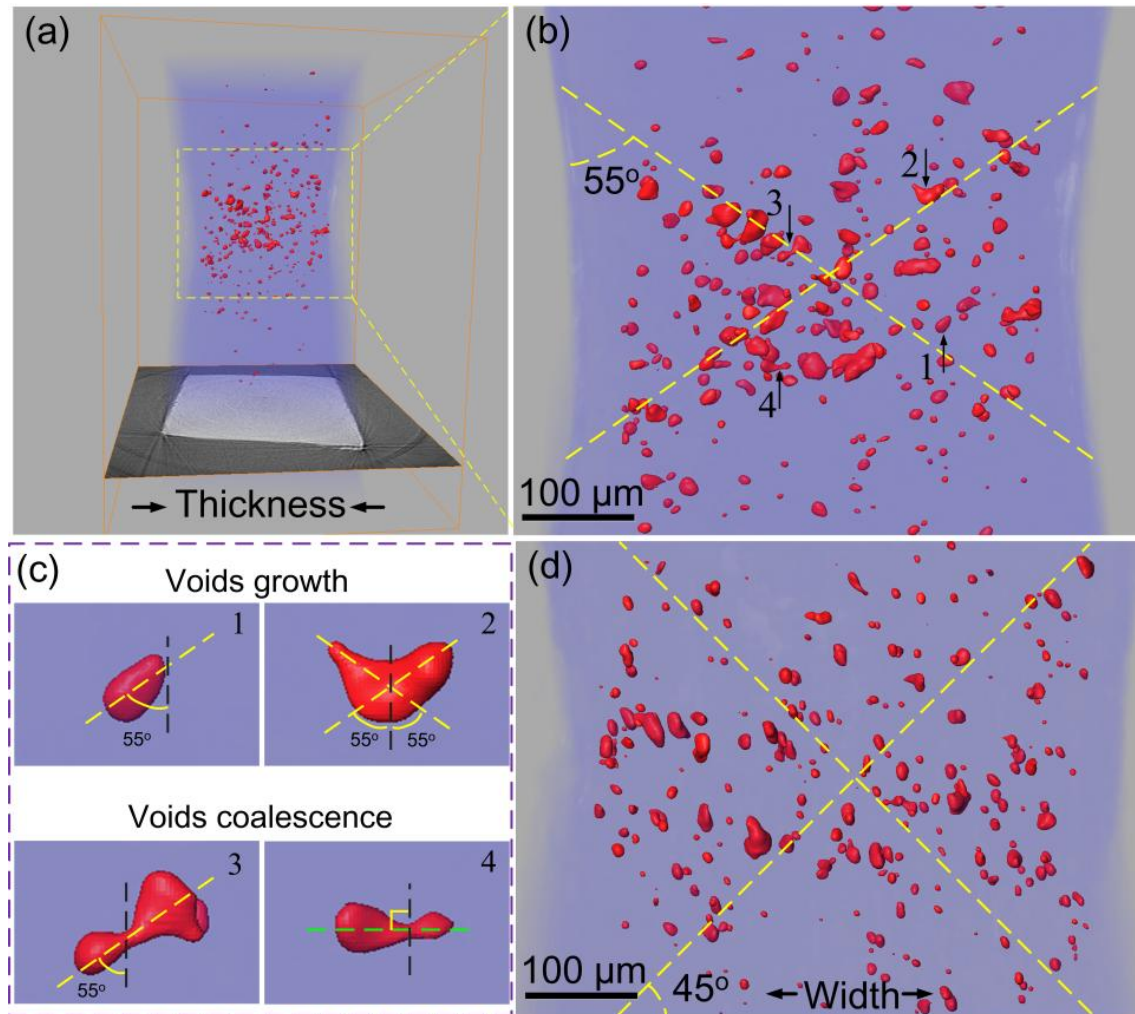


Figure 3. Volumetric reconstruction of the voids in the specimen after necking ( $\varepsilon \approx 0.22$ ) (a) the 3D image from the  $X$  (thickness) plane, (b) the necking zone showing partial enlargement of (a), (c) the classical voids growth and coalescence, and (d) from the  $Y$  (width) plane

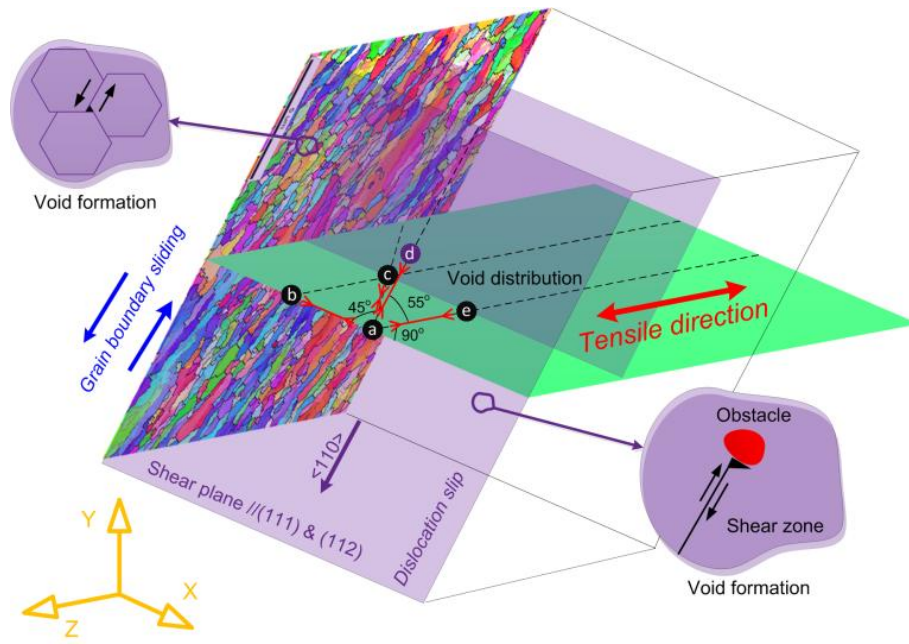


Figure 4. Schematic of the shear texture effect on the fracture behavior of UFG pure copper.